Bioorganic Chemistry 138 (2023) 106620

Contents lists available at ScienceDirect

Bioorganic Chemistry

journal homepage: www.elsevier.com/locate/bioorg

A multidisciplinary functional proteomics-aided strategy as a tool for the profiling of a novel cytotoxic thiadiazolopyrimidone

Elva Morretta [1], Dafne Ruggiero [1], Raffaella Belvedere, Antonello Petrella, Ines Bruno, Stefania Terracciano [*], Maria Chiara Monti [*]

Department of Pharmacy, University of Salerno, Via Giovanni Paolo II 132, 84084 Fisciano, Salerno, Italy

ARTICLE INFO

Keywords:
Thiadiazolopyrimidones
Heterocyclic scaffold
Functional proteomics
Protein-ligand interaction
Annexin A6

ABSTRACT

In recent years, thiadiazolopyrimidine derivatives have been acknowledged for their striking polypharmacological framework, thus representing an interesting scaffold for the development of new therapeutic candidates. This paper examines the synthesis and the interactome characterization of a novel bioactive thiadiazolopyrimidone (compound **1**), endowed with cytotoxic activity on HeLa cancer cells. In detail, starting from a small set of synthesized thiadiazolopyrimidones, a multi-disciplinary strategy has been carried out on the most bioactive one to disclose its potential biological targets by functional proteomics, using a label-free mass spectrometry based platform coupling Drug Affinity Responsive Target Stability and targeted Limited Proteolysis-Multiple Reaction Monitoring. The identification of Annexin A6 (ANXA6) as compound **1** most reliable cellular partner paved the way to deepen the protein–ligand interaction through bio-orthogonal approaches and to prove compound **1** action on migration and invasion processes governed by ANXA6 modulation. The identification of compund **1** as the first ANXA6 protein modulator represents a relevant tool to further explore the biological role of ANXA6 in cancer, as well as to develop novel anticancer candidates.

1. Introduction

Generally, in the drug discovery process, a large number of molecules are designed, filtered through appropriate *in-silico* techniques, synthesized, and biologically evaluated to identify new promising bioactive compounds that could be developed into novel therapeutics. Although considerable progress has been made, these approaches are time-consuming and costly and often lead to unsatisfactory results, particularly in terms of selectivity, side effects and toxicity, that limit the subsequent clinical stage.

To overcome these issues, different methods for an early target identification have been developed. For instance, during years, affinity chromatography coupled to mass spectrometry has been optimized to identify compound's biological targets, but it is limited by the need of the small molecule's derivatization, as many compounds cannot be modified without altering their binding specificity [1–4]. On another hand, genetic/genomic methods are limited to particular classes of compounds (e.g., those that influence transcription, localization, etc.) and, because they are based on downstream readouts, they do not necessarily identify primary targets [5].

Thus, new approaches are being established analyzing protein–drug interactions, such as Drug Affinity Responsive Target Stability (DARTS), which aims to discover the binding targets (and off-targets) of small molecules on a proteome-wide scale without the need to immobilize or modify it (e.g., by incorporation of biotin, fluorescent, radioisotope, or photoaffinity labels). DARTS is a relatively fast and simple approach, based on the protection against proteolysis conferred on the target protein by the interaction with the small molecule [6]. This method represents an excellent tool for the repositioning of different molecular platforms and/or for disclosing partners of newly synthesized bioactive compounds [7–9]. In this work, we used DARTS to disclose the interactome of the lead compound of a focused synthesized set of 7-methyl-5*H*-[1,3,4]thiadiazolo[3,2–*a*]pyrimidin-5-ones (**1**–**7**). Heterocyclic compounds represent a very attractive molecular platform in medicinal chemistry due to their chemical properties and the wide range of biological activities [10]. The thiadiazole ring, above all 1,2,4- and 1,3,4-

* Corresponding authors.
E-mail addresses: emorretta@unisa.it (E. Morretta), druggiero@unisa.it (D. Ruggiero), rbelvedere@unisa.it (R. Belvedere), apetrella@unisa.it (A. Petrella), brunoin@unisa.it (I. Bruno), sterracciano@unisa.it (S. Terracciano), mcmonti@unisa.it (M.C. Monti).
[1] These authors contributed equally to this work.

https://doi.org/10.1016/j.bioorg.2023.106620
Received 8 February 2023; Received in revised form 17 May 2023; Accepted 19 May 2023
Available online 20 May 2023

thiadiazoles, has emerged as an important framework for the development of antitumor, anti-inflammatory, anti-bacterial, anti-fungal, antiviral, anti-convulsant and anti-parasitic agents [10–15]. Several drugs containing thiadiazole are currently on the market: acetazolamide and methazolamide as diuretics, cefazoline sodium and cefazedone as the first generation of cephalosporins, timolol as a non-selective β-adrenergic receptor inhibitor [16,17]. Moreover, the thiadiazole ring, that acts as a bioisostere of pyrimidine, can interfere with the normal metabolism of nucleic acids. Because of the structural resemblance to adenine and guanine and their related derivatives, such as adenosine, guanosine, cAMP, cGMP and similar biomolecules, many thiadiazolopyrimidine scaffolds were developed and utilized by medicinal chemists to design novel therapeutics. In addition, condensed derivatives of thiazole core, such as thiazolo[4,5–d]pyrimidines and thiazolo[4,5–d] pyrimidinones, were reported to possess different biological profiles [15,18–21].

In this scenario, inspired by the potential of this class of heterocyclic compounds, we have focused our attention on a small set of [1,3,4] thiadiazolopyrimidones belonging to a large in-house collection, that can be easily synthesized exploiting a condensation reaction between the commercially available 2-amino-thiadiazoles and ethyl 3-oxobutanoate, as β-ketoester, in an acid medium. The scaffold was then decorated by Suzuki-Miyaura cross-coupling reaction which provided rapid access to different 2-arylated thiadiazolopyrimidones [19]. As part of a biological investigation on these molecules, a MTT assay was performed on HeLa cells, and it allowed us to identify compound **1** as the one characterized by the most interesting cytotoxic profile. Starting from this evidence, we decided to further investigate it by identifying its molecular interactors through DARTS based functional proteomics. Since compound **1** showed a very good interaction profile with some proteins, a deeper analysis has been performed using a multidisciplinary approach based on limited proteolysis assisted by mass spectrometry, biochemical and biophysical strategies followed by an *in-cell* investigation to prove the action mechanism of the selected compound.

2. Materials and methods

2.1. Synthesis of compounds 1–7

The starting reagents and solvents were purchased from Merck (Darmstadt, Germany). NMR spectra (^{1}H, ^{13}C) were recorded on Bruker Avance 400 MHz instrument, T = 298 K (Bruker, Milan, Italy). Coupling constants (*J*) are reported in Hertz, and chemical shifts are expressed in parts per million (ppm) on the delta (δ) scale relative to the solvent peak as the internal reference. Multiplicities are reported as follows: s, singlet; d, doublet; dd, doublet of doublets; ddd, doublet of doublet of doublets; t, triplet; dt, doublet of triplets; q, quartet; m, multiplet. Mass spectrometry experiments were performed using a Q-ToF™ Premiere instrument (Waters, Co®, Milan, Italy) or using an LTQ Orbitrap XL™ mass spectrometer (Thermo Scientific™, Monza, Italy) both equipped with an ESI source. The reactions were monitored on silica gel 60 F254 plates (Merck) and the spots were visualized under UV light (λ = 254 nm, 365 nm). Analytical and semi-preparative reversed-phase HPLC was performed on Agilent Technologies 1200 Series high-performance liquid chromatography using a Nucleodur, C8 reversed-phase column (75 × 4.6 mm, 5 μm, 80 Å, flow rate = 1 mL/min; 250 × 10.0 mm, 5 μm, 80 Å, flow rate = 4 mL/min respectively, Macherey Nagel®). The binary solvent system (A/B) was as follows: 0.1% TFA in water (A) and 0.1% TFA in CH_3CN (B). The absorbance was detected at 240 nm. All biologically tested compounds were determined to be > 97% pure by HPLC analysis and NMR data.

2.1.1. General procedure (A) for the synthesis of the intermediates II and III

5-(4-bromophenyl)-1,3,4-thiadiazol-2-amine (**a**) and 5-bromo-1,3,4-thiadiazol-2-amine (**b**) (1.0 equiv), respectively, ethyl 3-oxobutanoate **I** (1.3 equiv) and PPA (6.5 equiv) was heated on an oil bath at 160 °C for 1.5 h. The reaction mixture was poured into water and extracted with $CHCl_3$ (3 × 25 mL). The combined organic phases were washed with water (25 mL), dried over anhydrous Na_2SO_4, filtered, and concentrated in vacuum [22]. The desired compounds **II** and **III** were confirmed by analytical RP-HPLC (Nucleodur© C8 reversed-phase column: 75 × 4.6 mm, 5 μm, 80 Å, flow rate = 1 mL/min Macherey Nagel®), NMR and ESI-MS spectra and they were used for the next step without further purification.

2.1.2. 2-(4-bromophenyl)-7-methyl-5H-[1,3,4]thiadiazolo[3,2–a] pyrimidin-5-one (II)

Compound **II** was obtained by following the general procedure (**A**), from the reaction between **I** and 5-(4-bromophenyl)-1,3,4-thiadiazol-2-amine (**a**), as a brown solid (125 mg, 75% yield by HPLC analysis). RP-HPLC t_R = 30.1 min, gradient condition: from 5% B ending to 100% B 50 min, flow rate of 4 mL/min, λ = 240 nm. ^{1}H NMR (400 MHz, $(CD_3)_2SO$): δ_H = 7.96 – 7.93 (m, 2H), 7.87 – 7.84 (m, 2H), 6.35 (s, 1H). 2.32 (s, 3H). ESI-MS: calculated for $C_{12}H_8BrN_3OS$ 320.96; found *m/z* = 322.0189 $[M + H]^+$, 324.0190 $[M + H + 2]^+$.

2.1.3. 2-bromo-7-methyl-5H-[1,3,4]thiadiazolo[3,2–a]pyrimidin-5-one (III)

Compound **III** was obtained by following the general procedure (**A**), from the reaction between **I** and 5-bromo-1,3,4-thiadiazol-2-amine **(b),** as a brown solid (325 mg, 85% yield by HPLC analysis). RP-HPLC t_R = 15.7 min, gradient condition: from 5% B ending to 100% B 50 min, flow rate of 4 mL/min, λ = 240 nm. ^{1}H NMR (400 MHz, $(CD_3)_2SO$): δ_H = 6.30 (s, 1H), 2.28 (s, 3H). ESI-MS: calculated for $C_6H_4BrN_3OS$ 244.93; found *m/z* = 267.9120 $[M + Na]^+$, 269.9120 $[M + Na + 2]^+$.

2.1.4. General procedure (B) for the synthesis of 1–3

II (1.0 equiv), the correspondent boronic acid (**c-e**) (1.2 equiv), K_2CO_3 (2 equiv), and $Pd(PPh_3)_4$ (0.05 equiv) were placed in a two-neck round-bottom flask and fitted with a condenser. The system was evacuated and refilled with nitrogen five times. A mixture of dioxane/H_2O (rate 2:1) was placed in another 25 mL round-bottom flask, and five vacuum-nitrogen cycles were performed. Finally, dioxane/H_2O was added by a syringe in the flask with the powders and the mixture was refluxed overnight. Then, the reaction mixture was cooled, diluted with acidified water (20 mL), and filtered. The filtered was dried over anhydrous Na_2SO_4 and concentrated under vacuum [23]. The desired compounds **1**–**3** were confirmed by analytical RP-HPLC (Nucleodur© C8 reversed-phase column: 75 × 4.6 mm, 5 μm, 80 Å, flow rate = 1 mL/min Macherey Nagel®). HPLC purification was performed by semi-preparative reversed-phase HPLC (Nucleodur© C8 reversed-phase column: 250 × 10.0 mm, 5 μm, 80 Å, flow rate = 4 mL/min Macherey Nagel®). The final products were obtained with high purity (>98%) as detected by HPLC analysis and they were fully characterized by ESI-MS and NMR spectra.

2.1.5. 2-(5′-bromo-2′-ethoxy-[1,1′-biphenyl]-4-yl)-7-methyl-5H-[1,3,4] thiadiazolo[3,2–a]pyrimidin-5-one (1)

Compound **1** was obtained by following the general procedure (**B**), from the reaction between **II** and (5-bromo-2-ethoxyphenyl)boronic acid (**c**), as a brown solid (135 mg, 50% yield after HPLC purification). RP-HPLC t_R = 38.8 min, gradient condition: from 5% B ending to 100% B 50 min, flow rate of 4 mL/min, λ = 240 nm. ^{1}H NMR (400 MHz, CD_3OD): δ_H = 7.98 (dt, *J* = 8.7, 2.1 Hz, 2H), 7.67–7.62 (m, 2H), 7.42 – 7.36 (m, 2H), 6.94 (d, *J* = 8.6 Hz, 1H), 6.30 (s, 1H), 3.97 (q, *J* = 7.0 Hz, 2H), 2.36 (s, 3H), 1.29 (t, *J* = 7.0 Hz, 3H). ^{13}C NMR (100 MHz, $(CD_3)_2SO$): δ = 163.5, 161.8, 158.1, 156.5, 155.3, 141.5, 132.8, 132.6, 130.9, 130.8 (2C), 127.6 (2C), 127.5, 115.7, 112.7, 107.3, 64.6, 23.7, 14.9. ESI-MS: calculated for $C_{20}H_{16}BrN_3O_2S$ 441.01; found *m/z* = 442.0921 $[M + H]^+$, 444.0921 $[M + H + 2]^+$.

2.1.6. 4′-(7-methyl-5-oxo-5H-[1,3,4]thiadiazolo[3,2–a]pyrimidin-2-yl)-[1,1′-biphenyl]-4-carboxylic acid (2)

Compound **2** was obtained by following the general procedure (**B**), from the reaction between **II** and 4-carboxyphenylboronic acid (**d**), as a brown solid (80 mg, 60% yield after HPLC purification). RP-HPLC t_R = 22.3 min, gradient condition: from 5% B ending to 100% B 50 min, flow rate of 4 mL/min, λ = 240 nm. ^{1}H NMR (400 MHz, $(CD_3)_2SO$): δ_H = 8.05 (d, *J* = 8.0 Hz, 2H), 7.98 (d, *J* = 8,1 Hz, 2H), 7.93 – 7.86 (m, 4H), 5.63 (s, 1H), 2.13 (s, 3H). ^{13}C NMR (100 MHz, $(CD_3)_2SO$): *δ* = 198.8, 167.5, 160.3, 152.9, 149.6, 143.3, 142.3, 138.1, 130.7, 130.5 (2C), 129.0 (2C), 127.5 (2C), 127.3 (2C), 98.9, 18.7. ESI-MS: calculated for $C_{19}H_{13}N_3O_3S$ 363.39; found *m/z* = 364.1666 $[M + H]^+$.

2.1.7. 5-(4-(7-methyl-5-oxo-5H-[1,3,4]thiadiazolo[3,2–a]pyrimidin-2-yl) phenyl)furan-2-carbaldehyde (3)

Compound **3** was obtained by following the general procedure (**B**), from the reaction between **II** and 5-formyl-2-furanylboronic acid (**e**), as a brown solid (80 mg, 50% yield after HPLC purification). RP-HPLC t_R = 31.2 min, gradient condition: from 5% B ending to 100% B 50 min, flow rate of 4 mL/min, λ = 240 nm. ^{1}H NMR (400 MHz, $CDCl_3$): δ_H = 9.65 (s, 1H), 7.98 (dd, *J* = 8.5, 1.7 Hz, 2H), 7.90 (dd, *J* = 8.5, 1.7 Hz, 2H), 7.30 (dd, *J* = 3.8, 1.6 Hz, 1H), 6.95 (dd, 3.7, 1.6 Hz, 1H), 6.33 (s, 1H), 2.35 (s, 3H). ^{13}C NMR (100 MHz, $(CD_3)_2SO$): *δ* = 178.7, 163.6, 158.7, 158.4, 157.7, 156.5, 152.8, 132.7, 129.2, 128.8 (2C), 126.4 (2C), 125.5, 111.4, 107.3, 23.7. ESI-MS: calculated for $C_{17}H_{11}N_3O_3S$ 337.35; found *m/z* = 338.1346 $[M + H]^+$.

*2.1.8. General procedure (C) for the synthesis of **4–7***

A mixture of **III** (1.0 equiv), the appropriate arylboronic acids **f-i** (1.1 equiv), palladium(II)acetate (0.1 equiv), xantphos (0.2 equiv), and potassium carbonate (2.0 equiv) was vigorously stirred and heated in dry 1,4-dioxane (2 mL) at 100 °C for 16 h. Then, the reaction mixture was diluted with water and extracted with ethyl acetate. The organic layer was dried with Na_2SO_4 and the solvent was evaporated [24]. The desired compounds **5–8** were confirmed by analytical RP-HPLC (Nucleodur© C8 reversed-phase column: 75 × 4.6 mm, 5 μm, 80 Å, flow rate = 1 mL/min Macherey Nagel®). HPLC purification was performed by semi-preparative reversed-phase HPLC (Nucleodur© C8 reversed-phase column: 250 × 10.0 mm, 5 μm, 80 Å, flow rate = 4 mL/min Macherey Nagel®). The final products were obtained with high purity (>98%) as detected by HPLC analysis and were fully characterized by ESI-MS and NMR spectra.

2.1.9. 2-(2-methoxynaphthalen-1-yl)-7-methyl-5H-[1,3,4]thiadiazolo [3,2–a]pyrimidin-5-one (4)

Compound **4** was obtained by following the general procedure (**C**), from the reaction between **III** and 2-methoxy-1-naphthaleneboronic acid (**f**), as a brown solid (80 mg, 40% yield after HPLC purification). RP-HPLC t_R = 34.3 min, gradient condition: from 5% B ending to 100% B 50 min, flow rate of 4 mL/min, λ = 240 nm. ^{1}H NMR (400 MHz, $CDCl_3$): *δ* = 8.37 (dd, *J* = 8.7, 1.0 Hz, 1H), 7.99 (d, *J* = 9.1 Hz, 1H), 7.79–7.76 (m, 1H), 7.53 (ddd, *J* = 8.5, 6.8, 1.4 Hz, 1H), 7.38 (ddd, *J* = 8.0, 6.8, 1.1 Hz, 1H), 7.28 (d, *J* = 9.1 Hz, 1H), 6.29 (s, 1H), 3.97 (s, 3H), 2.36 (s, 3H). ^{13}C NMR (100 MHz, $CDCl_3$): *δ* = 163.6, 162.2, 157.3, 156.7, 154.9, 134.6, 132.0, 129.2, 128.8, 128.4, 124.8, 124.4, 112.1, 110.4, 107.0, 56.6, 24.0. ESI-MS: calculated for $C_{17}H_{13}N_3O_2S$ 323.07; found *m/z* = 346.0611 $[M + Na]^+$.

2.1.10. 2-(2,5-dimethoxyphenyl)-7-methyl-5H-[1,3,4]thiadiazolo[3,2–a] pyrimidin-5-one (5)

Compound **5** was obtained by following the general procedure (**C**), from the reaction between **III** and 2,5-dimethoxyphenylboronic acid (**g**), as a brown solid (65 mg, 50% yield after HPLC purification). RP-HPLC t_R = 31.8 min, gradient condition: from 5% B ending to 100% B 50 min, flow rate of 4 mL/min, λ = 240 nm. ^{1}H NMR (400 MHz, $CDCl_3$): δ_H = 7.86 (d, *J* = 3.1 Hz, 1H), 7.07 (dd, *J* = 9.1, 3.1 Hz, 1H), 6.95 (d, *J* = 9.1 Hz, 1H), 6.31 (s, 1H), 3.94 (s, 3H), 3.81 (s, 3H), 2.35 (s, 3H). ^{13}C NMR (100 MHz, $(CD_3)_2SO$): *δ* = 163.6, 162.3, 156,4, 153.9, 153.3, 152.1, 121.4, 117.4, 115.2, 110.8, 106.7, 57.4, 56.2, 23.8. ESI-MS: calculated for $C_{14}H_{13}N_3O_3S$ 303.34 found *m/z* = 304.0747 $[M + H]^+$, 326.0561 $[M + Na]^+$.

2.1.11. 7-methyl-2-(2-(trifluoromethoxy)phenyl)-5H-[1,3,4]thiadiazolo [3,2–a]pyrimidin-5-one (6)

Compound **6** was obtained by following the general procedure (**C**) from the reaction between **III** and 2-(trifluoromethoxy)phenylboronic acid (**h**), as a brown solid (70 mg, 75% yield after HPLC purification). RP-HPLC t_R = 34.8 min, gradient condition: from 5% B ending to 100% B 50 min, flow rate of 4 mL/min, λ = 240 nm. ^{1}H NMR (400 MHz, $CDCl_3$): *δ* = 8.41 (dd, *J* = 8.0, 1.7 Hz, 1H), 7.58 (ddd, *J* = 8.3, 7.4, 1.7 Hz, 1H), 7.44–7.36 (m, 2H), 6.29 (s, 1H), 2.34 (s, 3H). ^{13}C NMR (100 MHz, $(CD_3)_2SO$): *δ* = 163.8, 161.8, 156.4, 152.5, 146.3, 135.0, 130.4, 128.9, 121.9, 121.7, 119.0, 107.2, 23.7. ESI-MS: calculated for $C_{13}H_8F_3N_3O_2S$ 327.28 found *m/z* = 328.0354 $[M + H]^+$, 350.0171 $[M + Na]^+$.

2.1.12. 5-(dimethylamino)-N-(3-(7-methyl-5-oxo-5H-[1,3,4]thiadiazolo [3,2–a]pyrimidin-2-yl)phenyl)naphthalene-1-sulfonamide (7)

Compound **7** was obtained by following the general procedure (**C**), from the reaction between **III** and 3-(dansylamino)phenylboronic acid (**i**), as a brown solid (105 mg, 55% yield after HPLC purification). RP-HPLC t_R = 34.8 min, gradient condition: from 5% B ending to 100% B 50 min, flow rate of 4 mL/min, λ = 240 nm. ^{1}H NMR (400 MHz, $(CD_3)_2SO$): δ_H = 11.10 (s, 1H), 8.47 (dd, *J* = 8.4, 2.8 Hz, 1H), 8.38 (dd, *J* = 8.7, 2.7 Hz, 1H), 8.30 (dd, *J* = 7.4, 2.8 Hz, 1H), 7.68–7.62 (m, 3H), 7.49 (d, *J* = 7.5, 1H), 7.42 (d, *J* = 7.7 Hz, 1H), 7.36 (d, *J* = 8.0 Hz, 1H), 7.28 (dd, *J* = 7.7, 2.8 Hz, 1H). 6.32 (s, 1H), 2.81 (s, 6H), 2.30 (s, 3H). ^{13}C NMR (100 MHz, $(CD_3)_2SO$): *δ* = 163.5, 161.5, 157.7, 156.4, 151.9, 139.3, 134.7, 131.2, 131.0, 130.5, 129.5, 129.5, 129.4, 128.9, 124.1, 123.1, 122.5, 118.9, 116.5, 115.9, 107.3, 45.5 (2C), 23.7. ESI-MS: calculated for $C_{24}H_{21}N_5O_3S_2$ 491.11; found *m/z* = 492.1144 $[M + H]^+$, 514.0963 $[M + Na]^+$.

2.2. Cell line

Human cervical carcinoma HeLa cell line (Merck, Darmstadt, Germany) was cultured in Dulbecco's modified Eagle's medium (DMEM; Euroclone) containing 10% (v/v) fetal bovine serum (FBS, Thermo Fisher Scientific, Massachusetts, USA) supplemented with 10 U/ml penicillin and 0.01 mg/ml streptomycin (Euroclone, Milan, Italy). Cells were grown at 37 °C under a 5% CO_2 air-humidified atmosphere. To ensure logarithmic growth, the cells were sub cultured every 2 days. The cell line was tested for mycoplasma using PCR analysis.

2.3. Cell viability assay

Cell viability was determined by a MTT conversion assay (Merck, Darmstadt, Germany). HeLa were seeded in triplicate in 96 well-plates (3.5×10^3/well) and incubated for 72 h in the absence or presence of compounds **1–7** at a final concentration of 10 and 50 μM or DMSO 0.1% (v/v) in DMEM. Only for compound **1**, the cells were incubated with increasing concentrations (between 1 and 100 μM) for 24, 48, or 72 h or DMSO 0.1% (v/v) in DMEM. Stock solutions of compounds were stored at −20 °C and diluted just before addition to the sterile culture medium. Following the treatment, 20 μL of MTT solution (5 mg/mL in PBS) [3-4,5-dimethyldiazol-2-yl]-2,5-diphenyl tetrazolium bromide reagent (Sigma-Aldrich), was added, and the cells were incubated for an additional 4 h at 37 °C. The formazan crystals thus formed were dissolved in 100 μL of buffer containing 50% (v/v) N,*N*-dimethylformamide, 20% SDS (sodium dodecyl sulfate) (pH 4.5). The absorbance was measured at 550 nm with a Multiskan^{TM} GO Microplate Spectrophotometer (Thermo Fisher Scientific, Massachusetts, USA) [25].

2.4. Parallel artificial membrane permeability assay (PAMPA)

Compound **1** solution at 50 μM was used to perform PAMPA assay [26]. The permeability value *LogPe* has been determined as previously reported [27].

2.5. DARTS: Identification of compound 1 protein partners

HeLa cell pellets were lysed as reported by Morretta et al. [28]. Proteins aliquots (300 μg in 100 μL) were either treated with DMSO or increasing amounts of compound **1** (final concentrations: 0.5 μM, 5 μM and 50 μM; final DMSO at 1.6% vol/vol) and incubated for 1 h at room temperature. Samples were then submitted to limited proteolysis (1:500 w/w subtilisin to proteins ratio) for 30 min (25 °C, 450 rpm). An aliquot of the DMSO-treated lysate was submitted to mock proteolysis. Subtilisin was then quenched with 1 mM phenylmetane-sulfonil-fluoride (PMSF, Sigma Aldrich-Merck). This DARTS experiment was performed in triplicate.

Then, SDS PAGE runs, gel digestion, UHPLC-MS/MS and Proteome Discoverer (version 2.4.1.15) analysis were carried out as already reported [29,30].

Label-free quantification was performed by exploiting both unique and razor peptides for proteins abundance calculation, and a pairwise ratio-based approach was used to evaluate compound **1** *vs* ctrl proteins abundances. For each calculated ratio, a background-based *t*-test was performed.

2.6. Compound 1 protein partners validation through Western blotting

Western blotting analyses were carried out as reported by Ferraro et al. [31]. The following primary antibodies were used: anti-BiP (Cell Signaling, host rabbit, 1:1000 vol/vol), anti-mHMGCS, anti-ANXA6 and anti-ACSL3 (Santa Cruz Biotechnology Inc., host mouse, 1:250 vol/vol, 1:1000 vol/vol and 1:500 vol/vol, respectively) and then rabbit or mouse peroxidase-conjugated secondary antibodies were added (1:2500 vol/vol for rabbit and 1:500 vol/vol for mouse; Thermo-Scientific). Glyceraldehyde-3-Phosphate Dehydrogenase (GAPDH, Santa Cruz Biotechnology Inc., host mouse, 1:2000 vol/vol) was used as a loading normalizer.

2.7. Compound 1/ANXA6 interaction validation

For the determination of ANXA6 T_{agg} through thermal shift assay, HeLa cells were lysed as reported by Morretta et al. [28] and the protein concentration was adjusted to 3 μg/μl with PBS. Then, equal protein amounts were heated at different temperatures (from 37.2 °C to 72.1 °C) in a thermocycler (PEQSTAR, Euroclone) for 3 min, kept at 25 °C for 5 min and then centrifuged (21,000 g for 30 min at 4 °C) to pellet aggregated proteins. Each supernatant (5 μL) underwent Western blotting analysis as previously reported, using an anti-ANXA6 (1:500 vol/vol) antibody. T_{agg} was determined through *GraphPad Prism 7* (Supplementary Fig. S2). Subsequently, the same experiment was repeated incubating equal amounts of 3 μg/μl HeLa lysates with or without 50 μM compound **1** (final DMSO at 1.6% vol/vol) for 1 h at room temperature. Samples were then split into 50 μg aliquots and heated in the thermocycler at increasing temperatures until T_{agg} (39, 45.1, 49.1, 56.6 and 60.4 °C), as already reported. Samples were then centrifuged, and the supernatants (5 μL each) were submitted to Western blotting using anti-ANXA6 (1:500 vol/vol) and anti-GAPDH (1:2000 vol/vol) antibodies.

DARTS on the recombinant human ANXA6 (Sino Biological, Beijing, China) was performed as follows: 20 μL of a 10 ng/μl ANXA6 solution were incubated with either the vehicle or increasing compound **1** amounts (final concentrations: 0.5 μM, 5 μM and 50 μM; DMSO at 1.6% vol/vol) for 1 h at room temperature. The resulting samples were then submitted to subtilisin limited proteolysis (1:500 w/w enzyme to protein ratio), keeping an untreated ANXA6 aliquot undigested, as a reference. SDS-PAGE was then performed and the obtained gel was submitted to a Silver Staining protocol.

For the *in-cell* DARTS experiment, HeLa cells were seeded in duplicate in 6 well-plates (5×10^5 cells/well) and incubated for 4 h in presence of compound **1** at a final concentration of 50 μM or DMSO (0.1% v/v) in DMEM. After the treatment, the cells were detached with trypsin and centrifuged (1200 rpm for 5 min).

The obtained control and compound **1**-treated cell pellets were lysed, as already reported, and protein concentration was adjusted to 3 μg/μL with PBS. Then, equal protein amounts were submitted to limited proteolysis (1:2500, 1:1500, and 1:500 w/w subtilisin to proteins ratios) for 30 min at 25 °C and 450 rpm. An aliquot of both the control and compound **1**-treated lysate was submitted to mock proteolysis. Subtilisin was then quenched with 1 mM PMSF (10 min at 25 °C and 450 rpm) and 20 μg of each sample were resolved on a 12% SDS-PAGE and submitted to Western blotting as previously reported.

2.8. ANXA6 MRM method building

ANXA6 (UniProt Accession: P08133) tryptic peptides were selected through the data resource *Peptide Atlas* (https://db.systemsbiology.net/sbeams/cgi/PeptideAtlas) on its Human build and queried into the *complete Human SRM Atlas* (https://db.systemsbiology.net/sbeams/cgi/PeptideAtlas/GetTransitions) to obtain their best daughter ions. Thus, methods listing ANXA6 peptides and their three best fragments were obtained and tested onto a HeLa tryptic digest. HeLa cell lysate was submitted to an *in-solution* digestion protocol as reported by literature [8,32].

2.9. T-LiP-MRM: Compound 1/ANXA6 interaction features evaluation

HeLa cells proteome aliquots, obtained as previously reported, were incubated with DMSO or compound **1** (5 and 50 μM final concentrations), for 1 h at room temperature. The samples were then submitted to limited proteolysis with 1:500 and 1:1500 (w/w) subtilisin to proteins ratios. Subtilisin was then quenched, and the samples denatured to be submitted to in solution tryptic digestion and desalting, as already reported [8,32]. The samples were then injected into the UHPLC-ESI-MRM system and analyzed through the previously optimized MRM methods. The area of each ANXA6 tryptic peptide peak was measured using the Analyst Software (AB Sciex). Each sample was analyzed in triplicate. Compound **1**-treated *vs* untreated tryptic peptides areas ratios were calculated from the averages of the areas of each peptide and a *t*-test was performed to calculate the associated p-Values. For compound **1** altered peptides, XICs exemplificative of one out of three replicates are reported in Supplementary Fig. S4.

2.10. Surface plasmon resonance

SPR experiments were carried out on a Biacore T200 instrument (GE Healthcare) equipped with a research-grade carboxy-methyl dextran CM5 sensor chip (Cytiva, Marlborough, USA). Recombinant human Annexin A6 (ANXA6), purchased from Sino Biological (Beijing, China), was immobilized on a sensor chip surface (0.1 μg μL^{-1} in 10 mM CH_3COONa, 25 mM, pH 4.5) at a flow rate of 10 μL min^{-1} to obtain densities of 6–7 kRU. As a reference, a flow cell was activated via EDC/NHS and deactivated with ethanolamine but no protein was immobilized. Compound **1** was dissolved to obtain 10 mM solutions in 100% DMSO and diluted 1:20 (v/v) in HBS-P (HEPES Buffered Saline: 0.1 M $C_8H_{18}N_2O_4S$, 1.5 M NaCl, 0.5% v/v Surfactant P20, pH 7.4) containing 1 mM Ca^{2+} to a final DMSO concentration of 5.0% [33]. For the interaction analysis, compound **1** was injected in concentration series (1:1 dilution, 9 different concentrations) spanning from 0.39 to 100 μM. The concentration series were prepared in triplicates in 96-well plates. SPR experiments were performed at 25 °C, using a flow rate of 20 μL min^{-1}, with 90 s monitoring of association and 200 s monitoring of dissociation.

K_D values were determined using the BIA evaluation software performing a global fit of the double-referenced association and dissociation data to a 1:1 interaction model.

2.11. Wound healing assay

HeLa cells were seeded in a 12-well plastic plate at 1×10^5 cells per well and the wound healing assay was performed as reported in [34]. In detail, cells were incubated in the presence of compound **1** at 12.5 and 25 μM final concentrations. All experimental points were further treated with mitomycin C (10 μg/ml, Sigma Aldrich, St. Louis, MO, USA) to ensure the block of mitosis.

2.12. Invasion assay

Cell invasiveness through the coating of matrigel was analyzed by seeding cells in 350 μL of medium serum-free at a number of 4×10^4/insert in the upper chamber of the *trans*-well. Then, 1.4 mL of supplemented growth medium was added with or without compound **1** at 12.5 and 25 μM final concentrations for 24 h at 37 °C in a 5% CO_2-95% air-humidified atmosphere. The whole procedure was perfomed as reported in [35]. The number of migrated cells to the lower surface was counted in twelve random fields using an EVOS light microscope (10 ×) (Life Technologies Corporation, Carlsbad, CA, USA).

2.13. Confocal analysis

HeLa cells were treated with compound **1** at 6.25, 12.5 and 25 μM for 6 and 24 h. Then, they were fixed and treated as reported in [36]. Next, cells were incubated with mouse monoclonal anti-ANXA6 (1:100; Santa Cruz Biotechnologies, Dallas, TX, USA) over night at 4 °C. After two washing steps, cells were incubated with AlexaFluor anti-mouse 488 and anti-rabbit 555 (1:500; Molecular Probes) for 2 h at room temperature (RT). Nuclei were detected with Hoechst 33,342 (1:1000; Molecular Probes; OR, USA). The images were acquired using a Leica SP8 confocal microscope (Leica Microsystems, Wetzlar, Germany).

2.14. Fluo-4am assay

HeLa cells were trypsinized, washed, and placed in 1.5 mL tubes at 5×10^5/ml and then incubated with compound **1** (12.5 and 25 μM final concentrations) in PBS 1 × for 30 min at RT. Then, the intracellular Ca^{2+} concentrations [Ca^{2+}] were measured using the fluorescent Fluo-4 a.m. probe (Molecular Probes, Thermo Fisher Scientific, Waltham, MA, USA), as previously described [37]. The fluorescence in each sample was analyzed by a BD FACSCalibur cytometer (Becton Dickinson FACScan, Franklin Lakes, NJ, USA). The buffers used were PBS 1 × without Ca^{2+} and in presence of 5 mM Ca^{2+}.

2.15. Small interfering (si)RNA transfection

siRNA sequences against ANXA6 were purchased from Santa Cruz Biotechnology [38] and used at a final concentration of 10 nM. ANXA6-siRNAs were transfected using TransIT-X2® Dynamic Delivery System (MirusBio), according to the manufacturer instructions. Cells were harvested after 48 h from transfection. The analysis of calcium mobilisation and cell migration and invasion have been performed with transfected cells as reported above.

2.16. Statistical analyses

Statistical comparisons between groups were made using two-way ANOVA to compare experimental groups. ANOVA test was followed by the Tukey's multiple comparisons test. Differences were considered significant if $P < 0.05$.

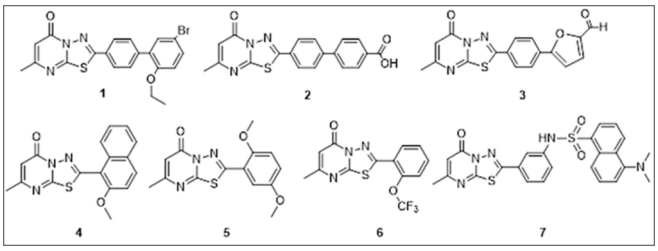

Fig. 1. Chemical structures of compounds **1**–**7**.

3. Results and discussion

3.1. Chemical synthesis

According to the procedure reported by Okabe, the pyrimidinones containing bisheterocycles were synthesized by exploiting a condensing ring-closure reaction [22]. Upon heating with polyphosphoric acid (PPA), the β-ketoesters and the appropriate heterocyclic amines were allowed to condense to give the pyrimido-heterocycles derivatives, likely through the initial imine formation which undergoes cyclization. In more detail, compound **1**–**7** (Fig. 1) were prepared by the synthetic route described in Scheme 1. Addition of the β-ketoesters **I** to commercially heterocyclic amines 5-(4-bromophenyl)-1,3,4-thiadiazol-2-amine (**a**) and 5-bromo-1,3,4-thiadiazol-2-amine (**b**) respectively, in presence of PPA at 140–160 °C for 1.5 h, afforded the intermediates **II** and **III,** respectively, in highly yield and purity (Scheme 1) [19]. The next synthetic step involved the Suzuki-Miyaura cross-coupling reaction which gives access to a further functionalization of the scaffold (Scheme 1) [39]. To obtain compounds **1**–**3**, **II** was placed to react with boronic acids **c-e** at reflux overnight in standard Suzuki coupling conditions: palladium(0) was used as catalyst, potassium carbonate as a base, and a mixture of 1,4-dioxane/water 2:1 as a solvent reaction [23]. To obtain compounds **4**–**7**, the intermediate **III** was placed to react at 100 °C for 16 h with the corresponding arylboronic acids (**f-i**) in presence of palladium(II)acetate, xantphos, a bidentate diphosphine ligand, and potassium carbonate using as solvent reaction dry 1,4-dioxane (Scheme 1) [24]. By using this procedure, compounds **1**–**7** were obtained quickly and in very good yields (Fig. 1 and Supplementary Figs. S6–S30).

3.2. Viability assay

To identify the most promising compounds within the set of synthesized thiadiazolopyrimidones, a preliminary cytotoxicity assay has been performed on HeLa cells, the most commonly used human carcinoma of the uterine cervix cell line. Compounds **1**–**7** were tested at two concentrations (10 and 50 μM) at 72 h (Fig. 2**A**). Compounds **1**, **5**, **6** and **7** showed a good antiproliferative effect, and our efforts were focused on compound **1** as it showed the best profile and it was able to induce a mortality rate of about 50% at 50 μM. Then, a cytotoxicity assay at 24, 48, and 72 h at different concentrations, ranging from 1.56 μM to 100 μM, was performed. Compound **1** showed a concentration-dependent antiproliferative activity after 72 h of incubation (Fig. 2**B**).

Next, to prove compound **1** permeability through membranes, a PAMPA assay has been performed showing a very good permeation profile with a logPe of −5.7697 (± 0.0098) at 50 μM.

3.3. Identification of compound 1 protein partners through DARTS

The identification of a promising item, compound **1**, and the absence of known biological targets driven us to accurately sought its protein partner(s), directly in a complex protein environment. Therefore, we submitted compound **1** to the first phase of our well established *label-free* functional proteomics platform, Drug Affinity Responsive Target Stability (DARTS). This method is based on the assumption that, when a

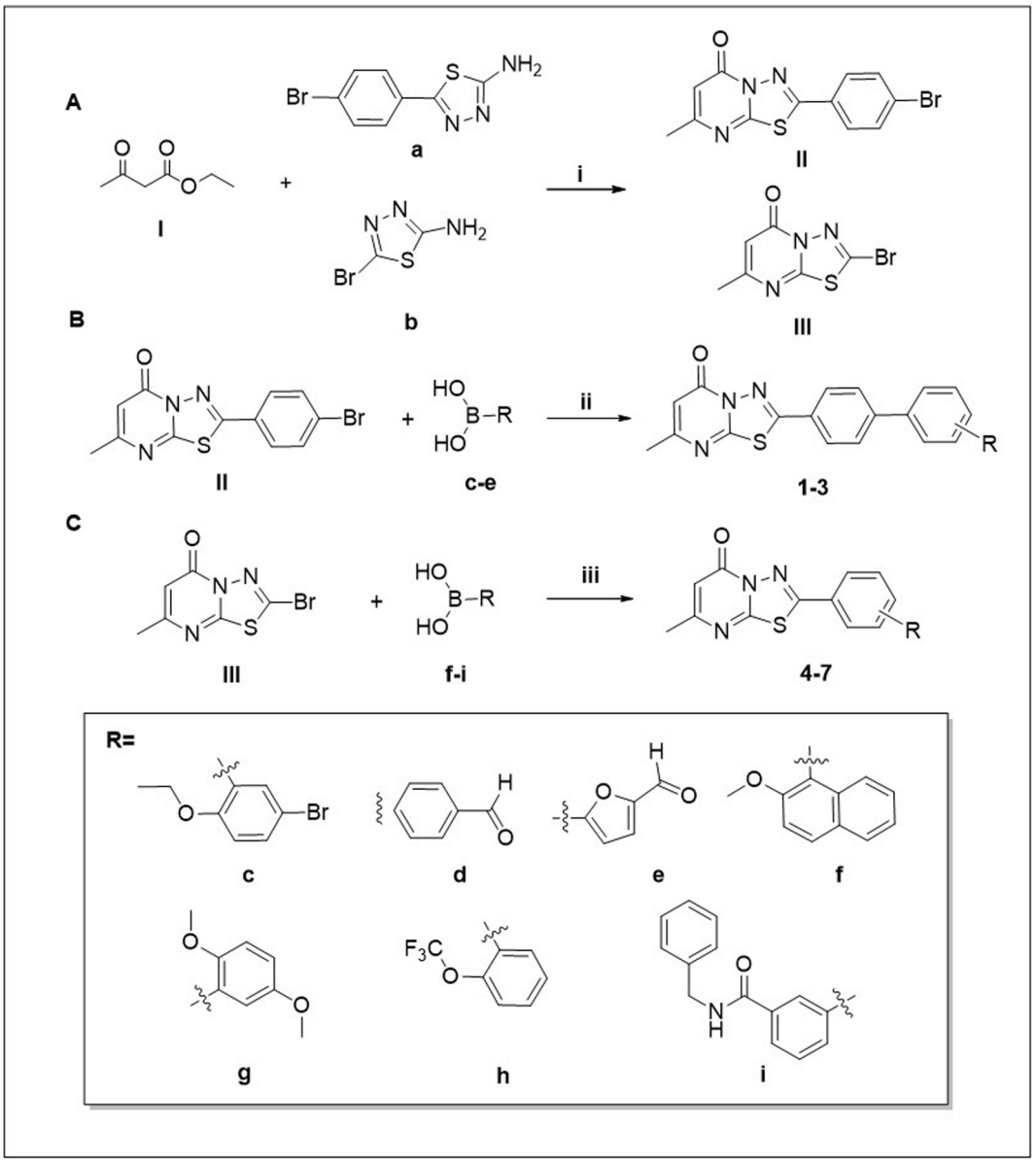

Scheme 1. Synthetic procedure for compounds **1**–**7**. Reagents and conditions: (**i**) PPA, 150 °C, 1.5 h; (**ii**) $Pd(PPh_3)_4$, K_2CO_3, dioxane/H_2O (2:1), reflux, overnight; (**iii**) $Pd(AcO)_2$, K_2CO_3, xantphos, dry 1,4-dioxane, 100 °C, 16 h.

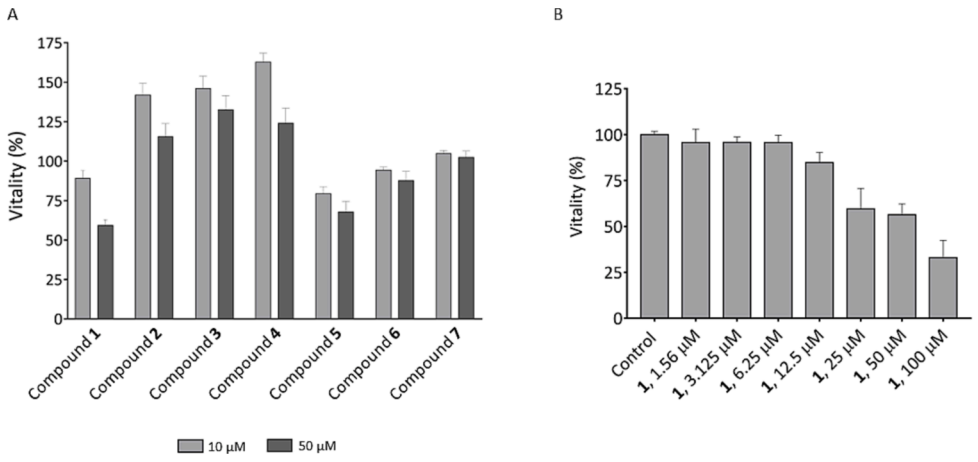

Fig. 2. (**A**) Antiproliferative activity of compounds **1**–**7** at 10 and 50 μM (light gray and dark gray bars, respectively) after 72 h of treatment on HeLa cells. (**B**) Antiproliferative activity on HeLa cells of compound **1** (from 1.56 to 100 μM) after 72 h of treatment.

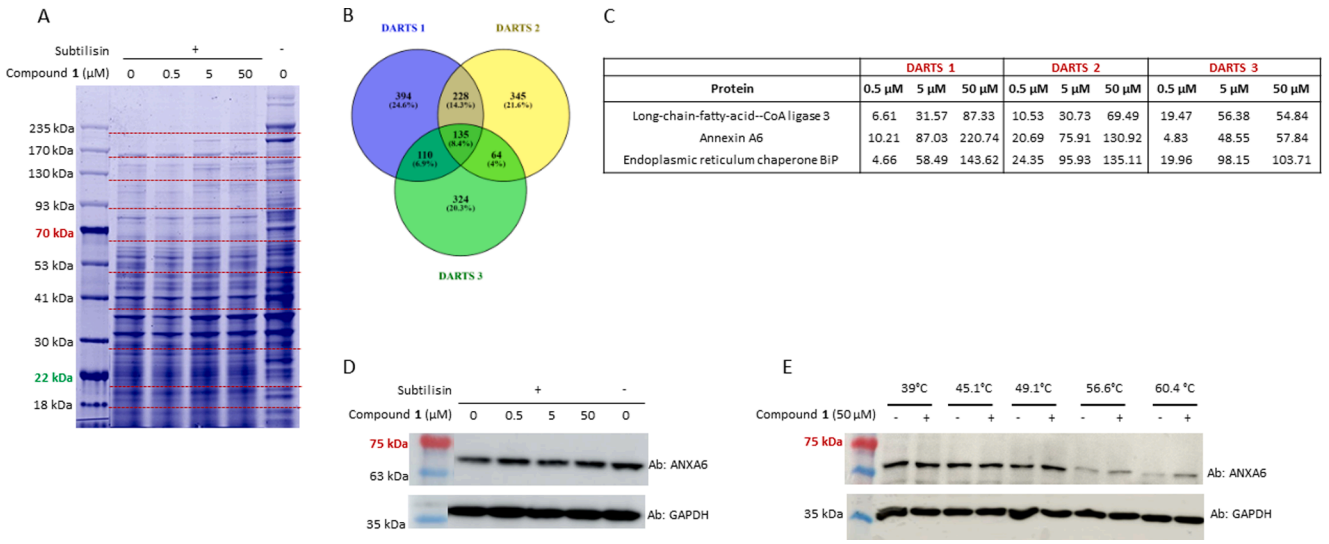

Protein	DARTS 1			DARTS 2			DARTS 3		
	0.5 μM	5 μM	50 μM	0.5 μM	5 μM	50 μM	0.5 μM	5 μM	50 μM
Long-chain-fatty-acid--CoA ligase 3	6.61	31.57	87.33	10.53	30.73	69.49	19.47	56.38	54.84
Annexin A6	10.21	87.03	220.74	20.69	75.91	130.92	4.83	48.55	57.84
Endoplasmic reticulum chaperone BiP	4.66	58.49	143.62	24.35	95.93	135.11	19.96	98.15	103.71

Fig. 3. (**A**) Coomassie stained SDS-PAGE of a DARTS experiment. The gel cutting pattern is denoted through red dotted lines. (**B**) Venn diagram reporting the numbers of identified proteins among three DARTS biological replicates. (**C**) Filtered list of compound **1** presumed partners, reported with their protection from proteolysis for the three biological replicates. The protection entity is reported as compound **1** *vs* control intensity ratio, expressed as a percentage of the lysate *vs* control which was set as 100%. (**D**) Western blotting analysis of a DARTS and (**E**) a TSA experiment. GAPDH has been used as a loading normalizer. (For interpretation of the references to colour in this figure legend, the reader is referred to the web version of this article.)

target binds its own ligand, it is stabilized in terms of protease exposure due to a conformational stabilization. The resistence to limited proteolysis, thus, can give infos about the direct partner of a small molecule in a cell lysate, observing the proteins after the proteolytic treatments via 1D-SDS-PAGE and classic *bottom-up* proteomics [8,9].

Thus, HeLa cell extracts, obtained in mild and non-denaturing conditions, were incubated with either compound **1** (0.5 μM, 5 μM, and 50 μM) or its vehicle, and then submitted to limited proteolysis with subtilisin. The mixtures were then run on an SDS-PAGE to detect protein bands whose intensity increased accordingly with compound **1** amount, due to its direct binding (Fig. 3**A**). Gels bands were submitted to an *in situ* tryptic digestion and to a nano-UHPLC-MS/MS analysis [29]. Proteins identification was achieved through the Proteome Discoverer software and is reported in Fig. 3**B**: 135 proteins were identified in three biological replicates and, among them, compound **1** putative interactors were disclosed via a *label-free* quantification. Indeed, protein intensities were calculated by Proteome Discoverer and compared *via* their ratios in treated *vs* untreated samples: compound **1** interactors were disclosed as those proteins whose intensities ratios increased in accordance with the small molecule amounts, in all of the independent DARTS experiments.

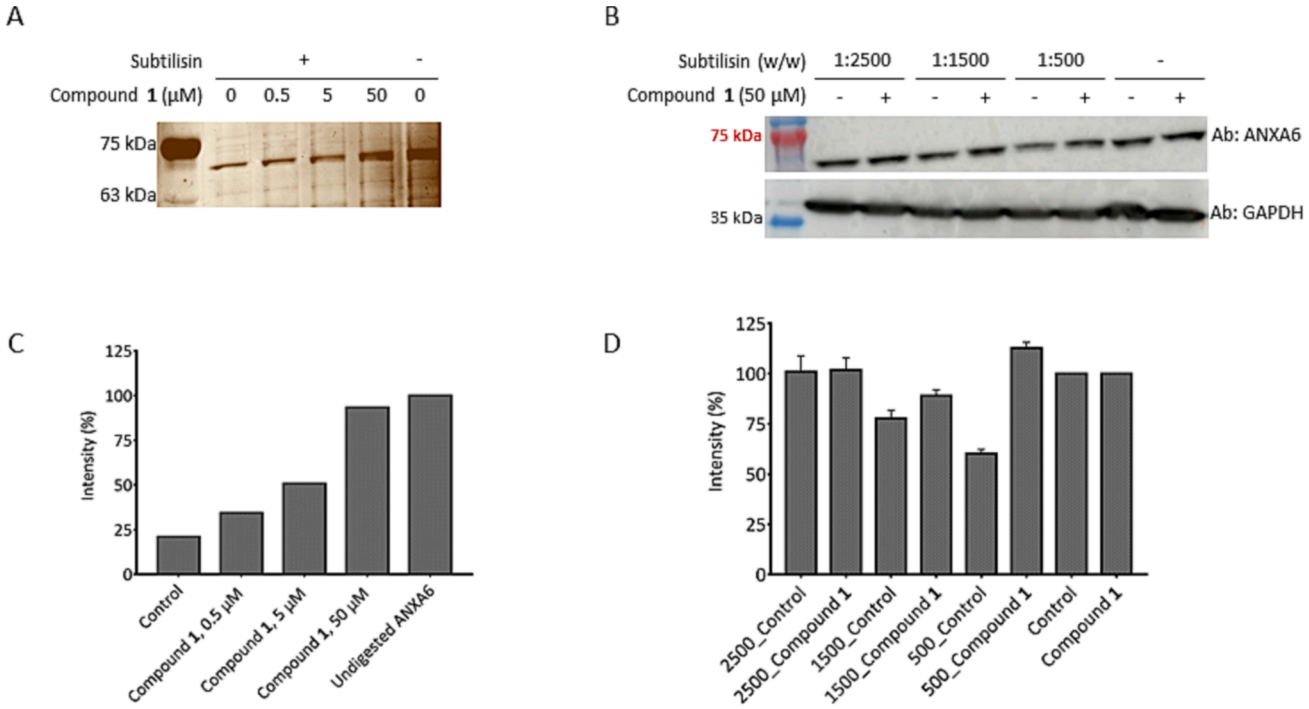

Fig. 4. (**A**) Silver stained SDS-PAGE of a DARTS experiment performed on isolated recombinant ANXA6, with (**C**) its relative densitometric analysis. (**B**) Western blotting analysis of the *in-cell* DARTS experiment. GAPDH has been used as a loading normalizer. The last two lanes show undigested ANXA6. (**D**) Densitometric analysis of panel B blot. Undigested ANXA6 (last two bars) was set as 100%.

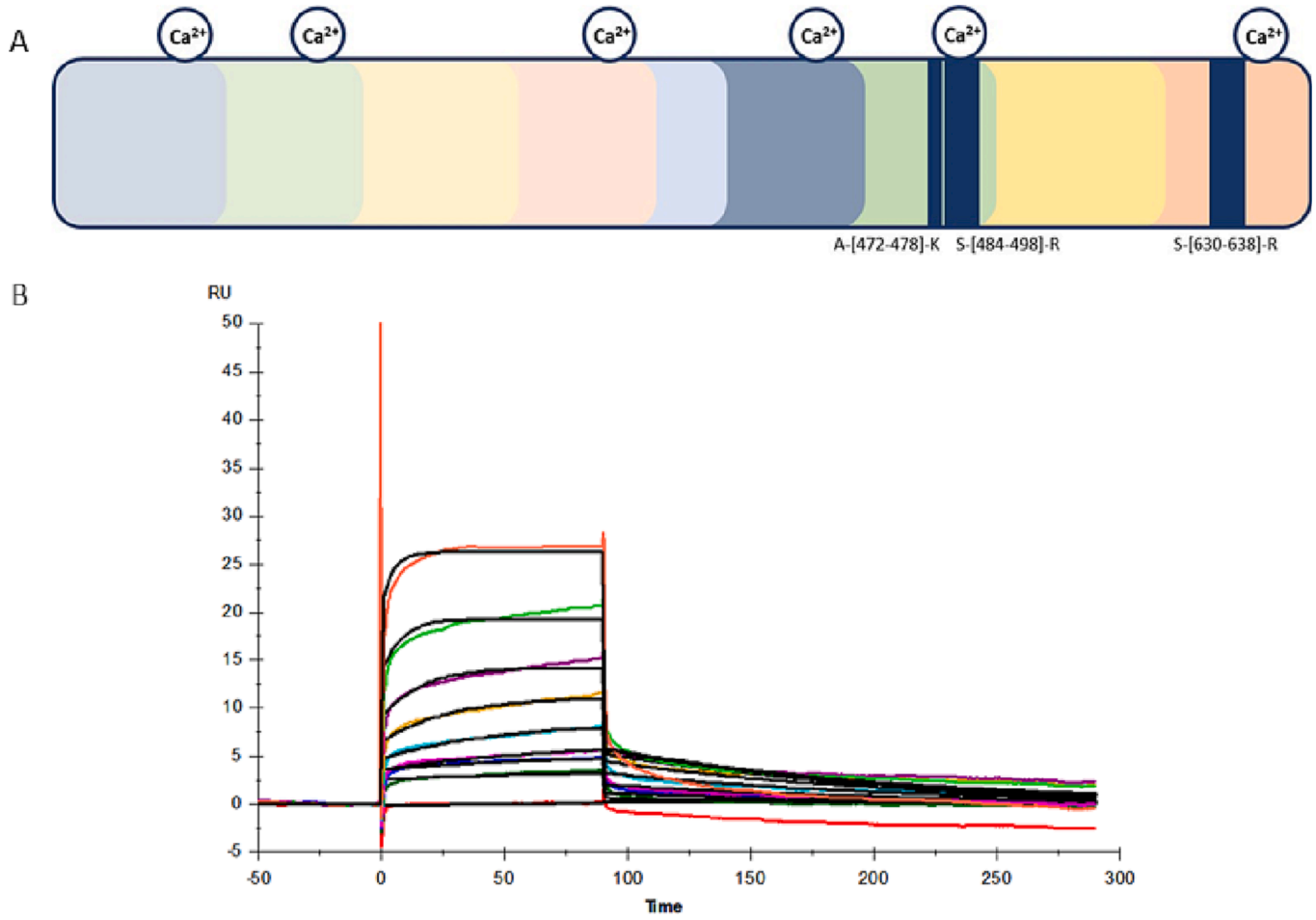

Fig. 5. (**A**) ANXA6 schematic representation showing the eight annexin repeats and the central linker region in different colors, as well as the six potential Ca^{2+} binding sites. Compound **1** protected peptides are indicated as blue bars and labeled with the corresponding amino acids numbering. (**B**) Compound **1** affinity for ANXA6 determination through Surface Plasmon Resonance. Compound **1** (red – 100 μM, light green – 50 μM, purple – 25 μM, brown – 12.5 μM, light blue – 6.25 μM, pink – 3.125 μM, blue – 1.56 μM, light green – 0.78 μM, dark orange – 0.39 μM) was passed over immobilized ANXA6 in the presence of 1 mM Ca^{2+} and the response units (RU) were plotted against time. (For interpretation of the references to colour in this figure legend, the reader is referred to the web version of this article.)

Only three proteins were protected by compound **1** in a concentration-dependent fashion: Long-chain-fatty-acid-CoA ligase 3 (i.e., ACSL3), Annexin A6 (i.e., ANXA6) and the endoplasmic reticulum chaperone BiP (i.e., BiP), as reported in Fig. 3**C**.

DARTS data were then validated by Western Blotting (Fig. 3**D** and Supplementary Fig. S1**A, C** and **E**), and their densitometric analyses (Supplementary Fig. S1**B, D** and **F**). As observable, BiP appeared to be consistently protected by compound **1** only at its highest concentration (Supplementary Fig. S1**E** and **F**), whereas ACSL3 (Supplementary Fig. S1**C** and **D**) and ANXA6 (Fig. 3**D** and Supplementary Fig. S1**A** and **B**) were strongly protected already at the lowest molecule amount, but only ANXA6 protection was concentration dependent. Thus, ANXA6 was considered compound **1** most consistent cellular partner. Furthermore, we moved on to perform a thermal stability assay (TSA) on HeLa cells lysates, to test wheter a perturbation event different from proteolysis confirmed the data for ANXA6. First, ANXA6 aggregation temperature (T_{agg}) was evaluated as being 59.43 ± 1.67 °C (Supplementary Fig. S2**A** and **B**), heating HeLa cells lysate aliquots at several temperatures. Then, the experiment was performed incubating the lysate with or without 50 μM compound **1** and heating the samples until the T_{agg} was reached, and results were revealed through Western blotting. As it can be observed, compound **1** induced ANXA6 thermal stabilization, clearly supporting its direct interaction with the protein (Fig. 3**E**).

As a further validation of compound **1** interaction with ANXA6, two additional DARTS experiments were also performed, one on the recombinant protein and one on compound **1**-treated HeLa cells. More in details, the first one was carried out incubating equal recombinant ANXA6 aliquots with increasing compound **1** amounts (i.e., 0.5, 5 and 50 μM), submitting the samples to subtilisin limited proteolysis and revealing the results by SDS-PAGE and silver staining. The obtained data are showed in Fig. 4**A** and **C**, confirming that compound **1** is able to protect isolated recombinant ANXA6 from subtilisin in a concentration dependent fashion.

The second one has been performed applying the same protocol on living cells: HeLa cells were incubated with 50 μM compound **1** or vehicle for 4 h and a DARTS experiment was performed. As observable in Fig. 4**B** and **D**, compound **1** was able to protect, also in a living system, the protein from proteolysis (at the subtilisin ratios of 1500 and 500 w/w). Moreover, it has to be noticed that it did not induce any variation in ANXA6 expression (panel **B**, last two lanes).

3.4. Compound 1/ANXA6 interaction features analysis: targeted limited proteolysis-multiple reaction monitoring

To additionally investigate compound **1** interaction with ANXA6, targeted limited proteolysis coupled with multiple reaction monitoring mass spectrometry (t-LiP-MRM) was performed. T-LiP-MRM is a *gel-free* approach that identifies protein region(s) directly involved with the molecule in the interaction process [32]. Indeed, when a compound interacts with a protein in a particular area, this region undergoes

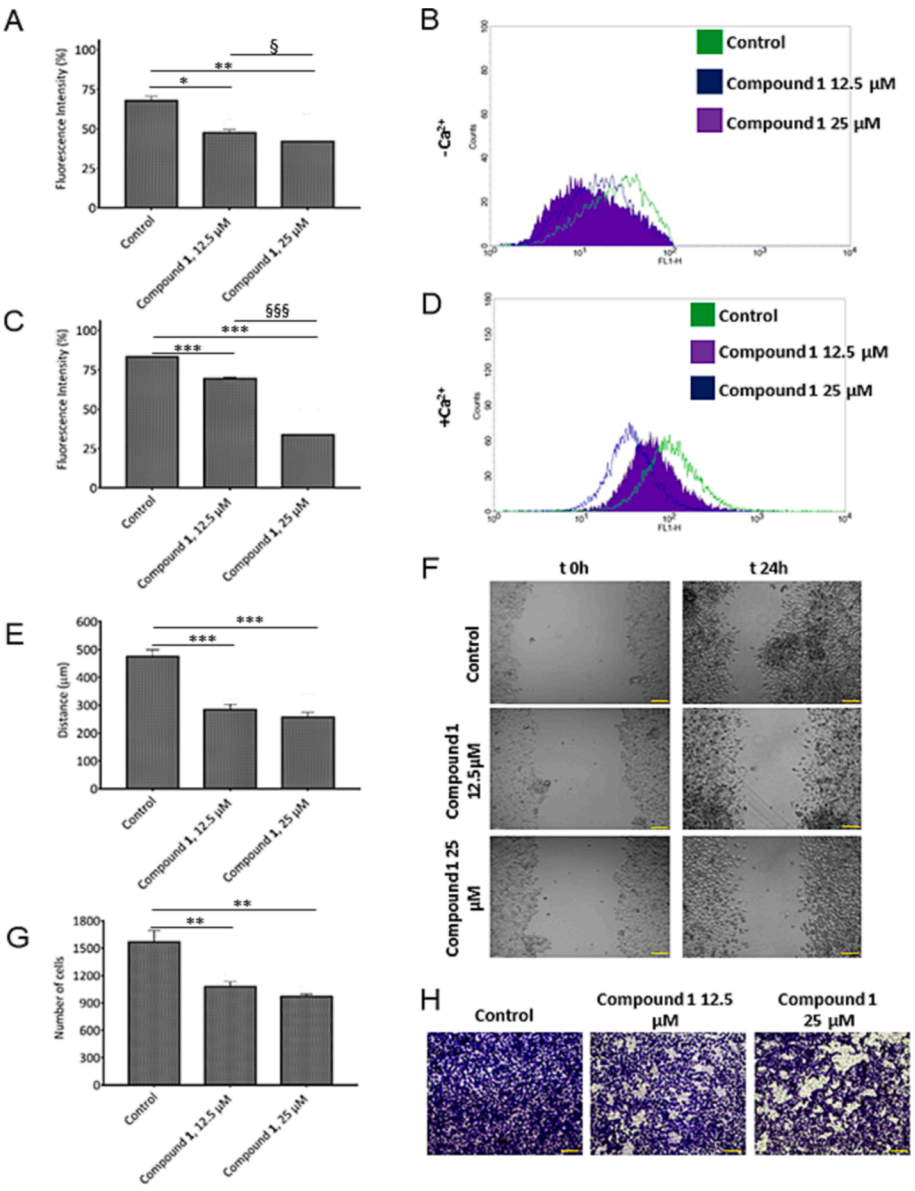

Fig. 6. Analysis of Ca^{2+} mobilization in HeLa cells. Effects of compound **1** at 12.5 and 25 µM were monitored using the probe Fluo-4 a.m for cyto-fluorimetric analysis (**A**) without $CaCl_2$ and (**C**) with 5 mM $CaCl_2$. In the related plots (**B** and **D** for $-Ca^{2+}$ and $+ Ca^{2+}$) green lines refer to the not treated cells, blue ones to compound **1** 12.5 µM, and purple area to 25 µM treatments. Evaluation of the migration (**E**) and invasion (**G**) speed of HeLa cells treated with compound **1** at 12.5 and 25 µM. Histograms and the related representative bright field images (**F** and **H**, for wound healing and invasion assays, respectively) are reported. Bar = 50 µm. Data represent the mean of three independent experiments ± SD with similar results. * $p < 0.05$; ** $p < 0.01$; *** $p < 0.001$ for treated cells *vs.* untreated controls; § $p < 0.05$; §§§ $p < 0.001$ for the point with compound **1** 25 µM *vs.* **1** 12,5 µM treatment. (For interpretation of the references to colour in this figure legend, the reader is referred to the web version of this article.)

conformational changes that modulate its sensitivity to limited proteolysis. Then, extensive tryptic digestion is performed, producing a mixture of semi-tryptic peptides (due to the previous subtilisin cuts) and fully-tryptic peptides (due to the undigested ones). The fully tryptic peptides are then quantified via MRM-mass spectrometry: their area will be higher if subtilisin-limited proteolysis is less effective due to the small molecule interaction [8].

Thus, a suitable MRM-MS method for ANXA6 was obtained by an *in silico* search: the protein fully tryptic peptides and their MRM transitions were obtained through *PeptideAtlas* and *SRMAtlas* and then analyzed on a HeLa tryptic digest. 42 peptidic signals and their most intense daughter ions were unequivocally recognized by UHPLC-MRM-MS and ANXA6 was mapped, obtaining a 70% sequence coverage (Supplementary Fig. S3, panel **A** and **B**, respectively).

Subsequently, HeLa lysate aliquots were incubated with compound **1** (5 and 50 µM) or vehicle (negative control) and submitted to the double digestion. An aliquot of the untreated sample was digested only with trypsin, to be kept as a lysate positive control. Peptides mixtures were then run on the UHPLC-MRM-MS system and the area of each ANXA6 tryptic peptide was quantified. Then, peptides mapping for ANXA6 regions sensitive to subtilisin (i.e., LiP peptides) were selected (lysate *vs* control areas ratios ≥ 1.5, p-Value ≤ 0.1) and examined in compound **1** treated samples: LiP peptides with an increased area in the samples exposed to the small molecule (ratios ≥ 1.5, p-Value ≤ 0.1) were considered symptomatic of compound **1** protection on specific ANXA6 region(s) (Supplementary Table S1). In particular, ANXA6 conformational changes due to compound **1** interaction were identified in its C-terminus, on the peptides 472–478, 484–498, and 630–638 (Fig. 5**A**, in dark blue).

3.5. Compound 1/ANXA6 interaction features analysis: SPR assay

A Surface Plasmon Resonance (SPR) assay was performed as an orthogonal test to deeply characterize the direct interaction between ANXA6 and compound **1**. Different concentrations of compound **1**, spanning from 0.39 µM to 100 µM, were injected on the target protein, a human recombinant full-length ANXA6, immobilized on the surface of the CM5 chip in presence of 1 mM Ca^{2+} [33]. The obtained results showed that compound **1** strongly binds the protein with a K_D in the low micromolar range ($K_D = 2.05 \pm 0.69$ µM) (Fig. 5**B** and Supplementary Fig. S31) [40].

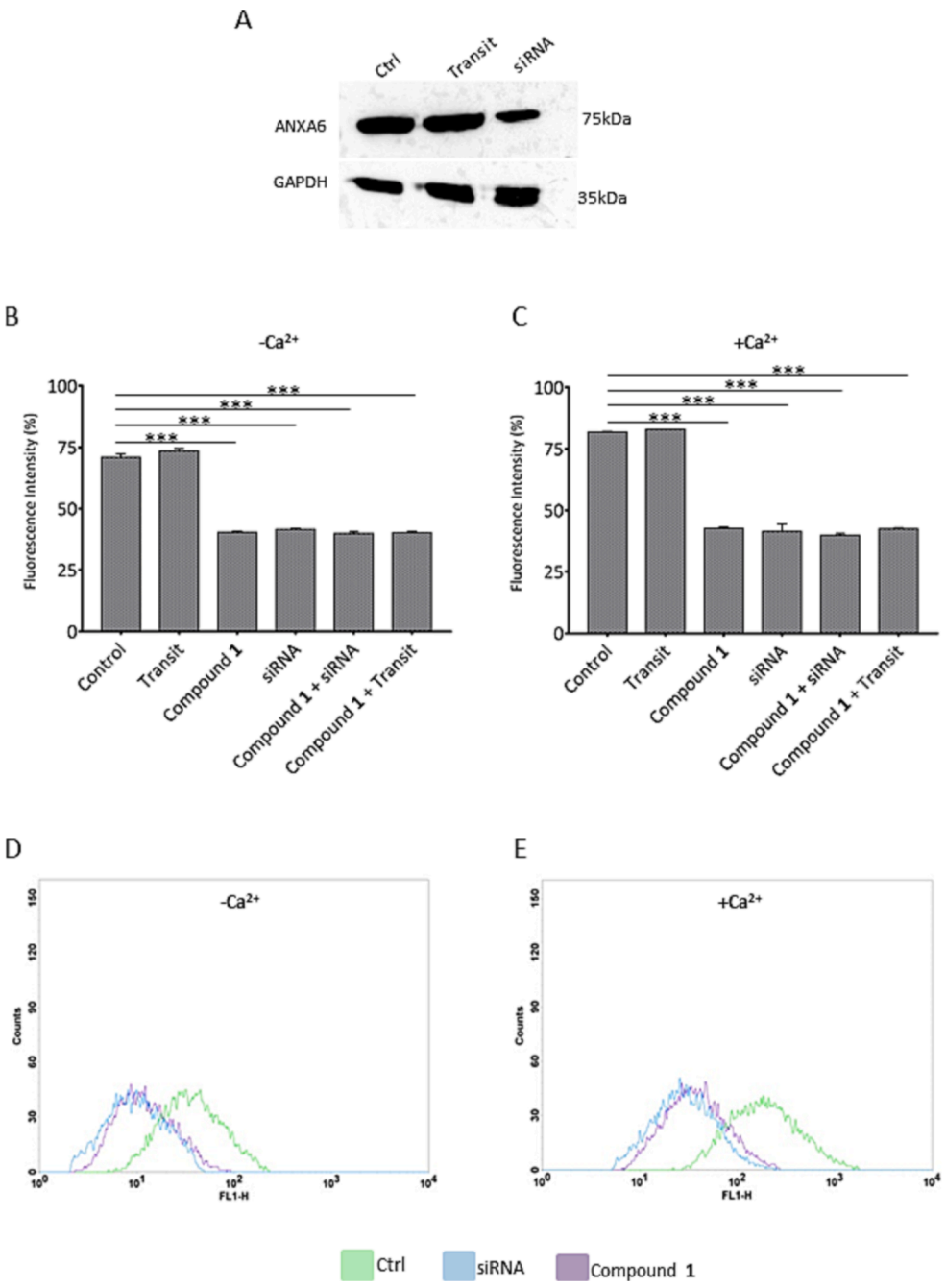

Fig. 7. (**A**) Western blot analysis on protein extracts from HeLa cells treated or not with siRNAs against ANXA6. Protein normalization was performed on GAPDH levels. Effects of 25 μM compound **1** and of 10 nM ANXA6 siRNA on calcium mobilization were monitored using the Fluo-4 a.m probe for cytofluorimetric analysis without (**B**) and with (**C**) 5 mM $CaCl_2$ in PBS 1x external buffer. In the representative plots (**D** and **E**, respectively), green lines refer to untreated cells, blue to ANXA6 siRNA and purple to 25 μM compound **1** treatment. (For interpretation of the references to colour in this figure legend, the reader is referred to the web version of this article.)

3.6. Compound 1 inhibits HeLa cells motility

Previous reports have demonstrated that ANXA6 strongly inhibits Ca^{2+} influx. In particular, the interference of this protein on the regulation of Ca^{2+} intracellular homeostasis is carried out through the reduction of the entry of this electrolyte across the plasma membrane and the decrease of its content in endoplasmic reticulum [41]. Once disclosed the interaction of compound **1** with ANXA6, we performed experiments in HeLa cells treating them with compound **1** at concentrations of 12.5 and 25 μM. First, we assessed calcium transition through the Fluo-4 a.m. cytofluorimetric assay. It has been shown that, both in absence and in presence of external calcium, compound **1** was able to inhibit the transition of this electrolyte in a concentration-dependent manner. In the two conditions, this effect appears evident as reported in histograms (Fig. 6**A** and **C**, in the absence and presence of calcium, respectively) and the representative plots generated by cytofluorimetric evaluation. Here, the control signal is represented by the green line, while the experimental points in presence of compound **1** at 12.5 μM and at 25 μM refer to the blue line and purple area, respectively (Fig. 6**B** and **D**, without and with calcium).

Next, we evaluated HeLa cell motility by analyzing the migration and invasion processes, since both of them are known to be particularly dependent on intracellular calcium mobilization [42]. Thus, we found that cell migration rate appeared notably inhibited, following a concentration-dependent effect after 24 h of treatment with compound **1** (Fig. 6**E** and **F**, for histogram analysis and representative bright field images, respectively). Moreover, the same trend has been found for the invasion process for which HeLa cells invaded the matrigel coating with a significantly lower speed in presence of compound **1** at 12.5 μM and even more at 25 μM (Fig. 6**G** and **H**, for histogram analysis and representative bright field images, respectively).

Interestingly, the confocal analysis performed on HeLa cells in

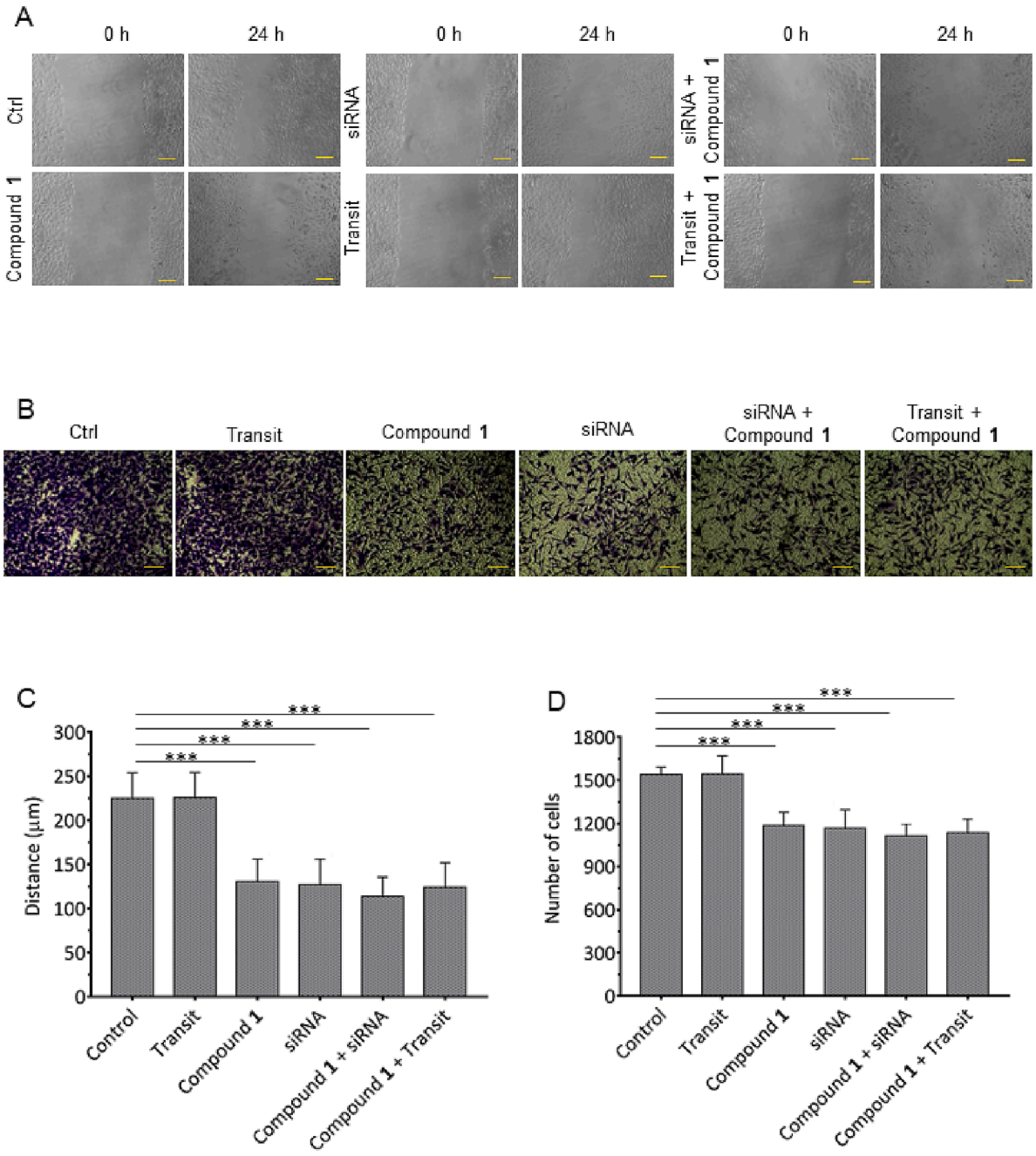

Fig. 8. Representative bright field images of the migration (**A**) and invasion (**B**) speed analysis of HeLa cells treated with 25 μM compound **1** for 24 h and ANXA6 siRNA for 48 h, reported with the corresponding bar graphs (**C** and **D**, for wound healing and invasion assays, respectively). Bar = 50 μm. Data represent the mean of three independent experiments ± SD with similar results. *** $p < 0.001$ for treated cells *vs* untreated controls.

presence of compound **1** at the three concentrations of 6.25, 12.5, and 25 μM for 6 and 24 h did not show any kind of differences in ANXA6 intracellular localization (see Supplementary Fig. S5).

3.7. Compound 1 biological effects closely resemble the knockdown of ANXA6 expression

In order to prove that compound **1** biological effects are mediated by its interaction with ANXA6, we induced its expression knockdown by transfecting HeLa cells with ANXA6 siRNAs. In Fig. 7**A**, the successful silencing of ANXA6 has been shown. Then, at 48 h from the transfection, the inhibition of calcium mobilization was assessed both in external absence and presence of this electrolyte, as shown in the bar graphs in Fig. 8**B** and **C**, respectively. Moreover, when compound **1** has been added to cells knocked down for ANXA6, no further significant effect has been revealed and in no case the transit (i.e., transfection agent) gave interference in the evaluated process. Moreover, the representative plots generated by cytofluorimetric evaluation in Fig. 8**D** and **E** showed the action of ANXA6 siRNA and of compound **1** in the buffer without or with calcium, with respect to the untreated cells.

Additionally, HeLa migration and invasion have been analyzed after 48 h from the transfection and 24 h from the administration of compound **1**. Once confirmed the inhibitory effects of the tested compound at a concentration of 25 μM, we highlighted that very similar negative actions are induced by silencing ANXA6 expression in both processes. These outcomes are reported in the bright field images in Fig. 8**A** and **B** for migration and invasion assays, respectively. The related histograms are shown in Fig. 8**C** and **D**. Also in these cases, the addition of

compound **1** on cell, already transfected with ANXA6 siRNA, did not provoke further changes. Moreover, transit did not induce any relevant effect.

4. Conclusions

The key purpose of this work was to determine the direct interactors of a novel synthetic cytotoxic thiadiazolopyrimidone in order to linkage its bioactivity to a well-defined biological pathway: the most likely targets of compound **1** have been inspected on HeLa cancer cells using a combination of proteomic strategies.

After the chemical synthesis, characterization and a raw biological evaluation, Drug Affinity Responsive Target Stability and targeted Limited Proteolysis combined to mass spectrometry were hired on the most active lead compound **1** and the results were validated by immunoblotting and SPR, as bio-orthogonal mass-spectrometry free techniques. The data suggested ANXA6 as the principal biological target for compound **1**, with a K_D in the low micromolar range, showing that ANXA6 C-terminal region was involved in the binding with the small molecule.

Annexins represent a wide and fascinating protein family with several functions important for cell motility. Each annexin encompasses a characteristic sequence at the *N*-terminus tracked by conserved repeats at C-terminal core, containing Ca^{2+} and phospholipid binding sites. ANXA6 belongs to this proteins group and it is widely recognized to be found at the plasma membrane and endosomal compartments, where it acts as a multi-functional protein recruiting signaling proteins, modulating cholesterol and membrane transport and influencing actin dynamics. Thus, ANXA6 is implicated in many biological processes, including cell proliferation, survival, differentiation and inflammation [43]. More recently, ANXA6 has been deeply studied for its involvement in cancer cell migration and invasion [44]. In fact, the temporary nature of Ca^{2+} spikes eases reversible membrane binding of ANXA6, making it suitable to induce protein complexes formation for a nonstop assembly and disassembly of specific machineries required for cellular movement.

In conclusion, since ANXA6 acts as an adhesion protein for migrating cells, small molecules, such as our promising compound **1**, could be of an enourmous pharmacological interest due to their ability of negatively modulate the aggressive migratory behavior of cancer cells, through a Ca^{2+} dependent mechanism. These findings define the effectivenes of our proposed functional proteomics-aidad approach, which allowed us to disclose the first synthetic ANXA6 small molecule modulator as an invaluable chemical probe and a potential anticancer therapeutic.

Funding

The work conducted in our laboratory and referred to in this paper was funded by University of Salerno (FARB 2020, 2021, 2022) and by POR Campania, FESR 2014/2020 (Asse 1—Obiettivo specifico 1.2—Azione 1.2) Project: Campania OncoTerapie CUP: B61G18000470007.

6. Institutional review board statement

Not applicable.

7. Informed consent statement

Not applicable.

8. Data availability statement

All relevant data are presented within the body of this paper.

9. Sample availability

Samples of some compounds are available from the authors.

CRediT authorship contribution statement

Elva Morretta: Methodology, Validation, Investigation, Writing – original draft. **Dafne Ruggiero:** Methodology, Validation, Investigation, Writing – original draft. **Raffaella Belvedere:** Methodology, Validation, Investigation, Writing – original draft. **Antonello Petrella:** Methodology, Writing – review & editing. **Ines Bruno:** Conceptualization, Methodology, Writing – review & editing. **Stefania Terracciano:** Conceptualization, Methodology, Writing – review & editing, Supervision. **Maria Chiara Monti:** Conceptualization, Methodology, Writing – review & editing, Supervision.

Declaration of Competing Interest

The authors declare that they have no known competing financial interests or personal relationships that could have appeared to influence the work reported in this paper.

Data availability

Data will be made available on request.

Appendix A. Supplementary data

Supplementary data to this article can be found online at https://doi.org/10.1016/j.bioorg.2023.106620.

References

[1] S. Ziegler, V. Pries, C. Hedberg, H. Waldmann, Target identification for small bioactive molecules: finding the needle in the haystack, Angew. Chem. Int. Ed. 52 (10) (2013) 2744–2792.
[2] Ong, S.-E.; Li, X.; Schenone, M.; Schreiber, S. L.; Carr, S. A., Identifying cellular targets of small-molecule probes and drugs with biochemical enrichment and SILAC. In *Chemical Proteomics*, Springer: 2012; pp 129-140.
[3] C. Cassiano, R. Esposito, A. Tosco, A. Zampella, M.V. D'Auria, R. Riccio, A. Casapullo, M.C. Monti, Heteronemin, a marine sponge terpenoid, targets TDP-43, a key factor in several neurodegenerative disorders, Chem. Commun. 50 (4) (2014) 406–408.
[4] F. del Gaudio, F. Pollastro, M. Mozzicafreddo, R. Riccio, A. Minassi, M.C. Monti, Chemoproteomic fishing identifies arzanol as a positive modulator of brain glycogen phosphorylase, Chem. Commun. 54 (91) (2018) 12863–12866.
[5] Y. Futamura, M. Muroi, H. Osada, Target identification of small molecules based on chemical biology approaches, Mol. Biosyst. 9 (5) (2013) 897–914.
[6] B. Lomenick, R.W. Olsen, J. Huang, Identification of direct protein targets of small molecules, ACS Chem. Biol. 6 (1) (2011) 34–46.
[7] Pai, M. Y.; Lomenick, B.; Hwang, H.; Schiestl, R.; McBride, W.; Loo, J. A.; Huang, J., Drug affinity responsive target stability (DARTS) for small-molecule target identification. In *Chemical biology*, Springer: 2015; pp 287-298.
[8] E. Morretta, R. Belvedere, A. Petrella, A. Spallarossa, F. Rapetti, O. Bruno, C. Brullo, M.C. Monti, Novel insights on the molecular mechanism of action of the anti-angiogenic pyrazolyl-urea GeGe-3 by functional proteomics, Bioorg. Chem. 115 (2021) 105168.
[9] E. Morretta, A. Sidibè, A. Spallarossa, A. Petrella, E. Meta, O. Bruno, M.C. Monti, C. Brullo, Synthesis, functional proteomics and biological evaluation of new 5-pyrazolyl ureas as potential anti-angiogenic compounds, Eur. J. Med. Chem. 226 (2021) 113872.
[10] Kumar, D.; Kumar, N. M.; Chang, K.-H.; Shah, K. J. E. j. o. m. c., Synthesis and anticancer activity of 5-(3-indolyl)-1, 3, 4-thiadiazoles. **2010,** *45* (10), 4664-4668.
[11] Badawey, E.; Rida, S.; Hazza, A.; Fahmy, H.; Gohar, Y. J. E. j. o. m. c., Potential anti-microbials. II. Synthesis and in vitro anti-microbial evaluation of some thiazolo [4, 5-d] pyrimidines. **1993,** *28* (2), 97-101.
[12] Kuppast, B.; Spyridaki, K.; Lynch, C.; Hu, Y.; Liapakis, G.; E Davies, G.; Fahmy, H. J. M. c., Synthesis of new thiazolo [4, 5-d] pyrimidines as corticotropin releasing factor modulators. **2015,** *11* (1), 50-59.
[13] S.M. Rida, N.S. Habib, E.A. Badawey, H.T. Fahmy, H.A. Ghozlan, Synthesis of novel thiazolo [4, 5-d] pyrimidine derivatives for antimicrobial, anti-HIV and anticancer investigation, Pharmazie 51 (12) (1996) 927–931.
[14] H.T.Y. Fahmy, S.A.F. Rostom, M.N. Saudi, J.K. Zjawiony, D.J. Robins, Synthesis and in vitro evaluation of the anticancer activity of novel fluorinated thiazolo [4, 5-d] pyrimidines, Archiv der Pharmazie: Int. J. Pharmaceut. Med. Chem. 336 (4–5) (2003) 216–225.

[15] A.A. Bekhit, H.T.Y. Fahmy, S.A.F. Rostom, A.M. Baraka, Design and synthesis of some substituted 1H-pyrazolyl-thiazolo [4, 5-d] pyrimidines as anti-inflammatory–antimicrobial agents, Eur. J. Med. Chem. 38 (1) (2003) 27–36.
[16] Masereel, B.; Rolin, S.; Abbate, F.; Scozzafava, A.; Supuran, C. T. J. J. o. m. c., Carbonic anhydrase inhibitors: anticonvulsant sulfonamides incorporating valproyl and other lipophilic moieties. **2002,** *45* (2), 312-320.
[17] M.T. Rabkin, E.W. Frederick, M. Lotz, L.H. Smith, Pyrimidine metabolism in man. v. the measurement in vivo of the biochemical effect of antineoplastic agents in animal and human subjects, J. Clin. Invest. 41 (4) (1962) 871–883.
[18] T.M. Salimov, M.A. Kukaniev, I.T. Sattorov, D.M. Osimov, Synthesis and Antimicrobial Activity of 2-Bromo-7-methyl-5-oxo-5H-1, 3, 4-thiadiazolo [3, 2-a] pyrimidine, Pharm. Chem. J. 39 (6) (2005) 311–312.
[19] B. Jafari, M. Ospanov, S.A. Ejaz, N. Yelibayeva, S.U. Khan, S.T. Amjad, S. Safarov, Z.A. Abilov, M.Z. Turmukhanova, S.N. Kalugin, 2-Substituted 7-trifluoromethyl-thiadiazolopyrimidones as alkaline phosphatase inhibitors. Synthesis, structure activity relationship and molecular docking study, Eur. J. Med. Chem. 144 (2018) 116–127.
[20] M.A. Kukaniev, T.M. Salimov, M.S. Murvatulloeva, I.K. Imatshoev, Reactions of thioamides and alkali metal salts of dithiocarbamates with 2-bromo-7-methyl-5-oxo-5H-1, 3, 4-thiazolo [3, 2-a] pyrimidine and antimicrobial activity of products, Pharm. Chem. J. 40 (8) (2006) 421–423.
[21] B. Kuppast, K. Spyridaki, C. Lynch, Y. Hu, G. Liapakis, E. Davies, G., Fahmy, H.,, Synthesis of new thiazolo [4, 5-d] pyrimidines as corticotropin releasing factor modulators, Med. Chem. 11 (1) (2015) 50–59.
[22] T. Okabe, K. Maekawa, E. Taniguchi, Syntheses of thiadiazolopyrimidine and related compounds, Agric. Biol. Chem. 37 (5) (1973) 1197–1201.
[23] S. Di Micco, L. Pulvirenti, I. Bruno, S. Terracciano, A. Russo, M.C. Vaccaro, D. Ruggiero, V. Muccilli, N. Cardullo, C. Tringali, R. Riccio, G. Bifulco, Identification by Inverse Virtual Screening of magnolol-based scaffold as new tankyrase-2 inhibitors, Bioorg. Med. Chem. 26 (14) (2018) 3953–3957.
[24] B. Jafari, N. Yelibayeva, M. Ospanov, S.A. Ejaz, S. Afzal, S.U. Khan, Z.A. Abilov, M. Z. Turmukhanova, S.N. Kalugin, S. Safarov, J. Lecka, J. Sévigny, Q. Rahman, P. Ehlers, J. Iqbal, P. Langer, Synthesis of 2-arylated thiadiazolopyrimidones by Suzuki-Miyaura cross-coupling: A new class of nucleotide pyrophosphatase (NPPs) inhibitors, RSC Adv. 6 (109) (2016) 107556–107571.
[25] S. Di Micco, S. Terracciano, D. Ruggiero, M. Potenza, M.C. Vaccaro, K. Fischer, O. Werz, I. Bruno, G. Bifulco, Identification of 2-(thiophen-2-yl) acetic Acid-Based Lead Compound for mPGES-1 Inhibition, Front. Chem. 9 (2021), 676631.
[26] G. Ferraro, R. Belvedere, A. Petrella, A. Tosco, B. Stork, S. Salamone, A. Minassi, F. Pollastro, E. Morretta, M.C. Monti, Drug affinity-responsive target stability unveils filamins as biological targets for artemetin, an anti-cancer flavonoid, Front. Mol. Biosci. 9 (2022).
[27] C. Festa, C. Finamore, S. Marchianò, F.S. Di Leva, A. Carino, M.C. Monti, F. del Gaudio, S. Ceccacci, V. Limongelli, A. Zampella, S. Fiorucci, S. De Marino, Investigation around the oxadiazole core in the discovery of a new chemotype of potent and selective FXR antagonists, ACS Med. Chem. Lett. 10 (4) (2019) 504–510.
[28] E. Morretta, A. Tosco, C. Festa, M. Mozzicafreddo, M.C. Monti, A. Casapullo, Crellastatin A, a PARP-1 Inhibitor Discovered by Complementary Proteomic Approaches, ChemMedChem 15 (3) (2020) 317–323.
[29] A. Shevchenko, H. Tomas, J. Havli, J.V. Olsen, M. Mann, In-gel digestion for mass spectrometric characterization of proteins and proteomes, Nat. Protoc. 1 (6) (2006) 2856–2860.
[30] S. Ceccacci, J. Deitersen, M. Mozzicafreddo, E. Morretta, P. Proksch, S. Wesselborg, B. Stork, M.C. Monti, Carbamoyl-phosphate synthase 1 as a novel target of phomoxanthone A, a bioactive fungal metabolite, Biomolecules 10 (6) (2020) 846.
[31] G. Ferraro, M. Mozzicafreddo, R. Ettari, L. Corsi, M.C. Monti, A Proteomic Platform Unveils the Brain Glycogen Phosphorylase as a Potential Therapeutic Target for Glioblastoma Multiforme, Int. J. Mol. Sci. 23 (15) (2022) 8200.
[32] S. Schopper, A. Kahraman, P. Leuenberger, Y. Feng, I. Piazza, O. Müller, P. J. Boersema, P. Picotti, Measuring protein structural changes on a proteome-wide scale using limited proteolysis-coupled mass spectrometry, Nat. Protoc. 12 (11) (2017) 2391–2410.
[33] Poeter, M.; Radke, S.; Koese, M.; Hessner, F.; Hegemann, A.; Musiol, A.; Gerke, V.; Grewal, T.; Rescher, U. J. B. e. B. A.-M. C. R., Disruption of the annexin A1/S100A11 complex increases the migration and clonogenic growth by dysregulating epithelial growth factor (EGF) signaling. **2013,** *1833* (7), 1700-1711.
[34] R. Belvedere, E. Pessolano, A. Porta, A. Tosco, L. Parente, F. Petrella, M. Perretti, A. Petrella, Mesoglycan induces the secretion of microvesicles by keratinocytes able to activate human fibroblasts and endothelial cells: A novel mechanism in skin wound healing, Eur. J. Pharmacol. 869 (2020) 172894.
[35] P. Franco, R. Belvedere, E. Pessolano, S. Liparoti, R. Pantani, A. Petrella, I. De Marco, PCL/Mesoglycan devices obtained by supercritical foaming and impregnation, Pharmaceutics 11 (12) (2019) 631.
[36] R. Belvedere, P. Saggese, E. Pessolano, D. Memoli, V. Bizzarro, F. Rizzo, L. Parente, A. Weisz, A. Petrella, miR-196a is able to restore the aggressive phenotype of annexin A1 knock-out in pancreatic cancer cells by CRISPR/Cas9 genome editing, Int. J. Mol. Sci. 19 (7) (2018) 1967.
[37] R. Belvedere, E. Morretta, N. Novizio, S. Morello, O. Bruno, C. Brullo, A. Petrella, The Pyrazolyl-Urea Gege3 Inhibits the Activity of ANXA1 in the Angiogenesis Induced by the Pancreatic Cancer Derived EVs, Biomolecules 11 (12) (2021) 1758.
[38] J. Bandorowicz-Pikuła, The roles of annexins in vascular endothelium dysfunction accompanying diabetes mellitus type 2, Postępy Biochemii 63 (2) (2017) 119–124.
[39] N. Miyaura, K. Yamada, A. Suzuki, A new stereospecific cross-coupling by the palladium-catalyzed reaction of 1-alkenylboranes with 1-alkenyl or 1-alkynyl halides, Tetrahedron Lett. 20 (36) (1979) 3437–3440.
[40] D. Ruggiero, S. Terracciano, G. Lauro, M. Pecoraro, S. Franceschelli, G. Bifulco, I. Bruno, Structural Refinement of 2, 4-Thiazolidinedione Derivatives as New Anticancer Agents Able to Modulate the BAG3 Protein, Molecules 27 (3) (2022) 665.
[41] K. Monastyrskaya, E.B. Babiychuk, A. Hostettler, P. Wood, T. Grewal, A. Draeger, Plasma membrane-associated annexin A6 reduces Ca2+ entry by stabilizing the cortical actin cytoskeleton, J. Biol. Chem. 284 (25) (2009) 17227–17242.
[42] C. Enrich, C. Rentero, S.V. de Muga, M. Reverter, V. Mulay, P. Wood, M. Koese, T. Grewal, Annexin A6—Linking Ca2+ signaling with cholesterol transport. *Biochimica et Biophysica Acta (BBA)-Molecular*, Cell Res. 1813 (5) (2011) 935–947.
[43] T. Grewal, M. Hoque, J.R.W. Conway, M. Reverter, M. Wahba, S.S. Beevi, P. Timpson, C. Enrich, C. Rentero, Annexin A6—A multifunctional scaffold in cell motility, Cell Adh. Migr. 11 (3) (2017) 288–304.
[44] O.Y. Korolkova, S.E. Widatalla, S.D. Williams, D.S. Whalen, H.K. Beasley, J. Ochieng, T. Grewal, A.M. Sakwe, Diverse roles of Annexin A6 in triple-negative breast cancer diagnosis, prognosis and EGFR-targeted therapies, Cells 9 (8) (2020) 1855.